Mon. Not. R. Astron. Soc. **377,** 1588–1596 (2007) doi:10.1111/j.1365-2966.2007.11710.x

The composition of Saturn's E ring

Jon K. Hillier,[1⋆] S. F. Green,[1] N. McBride,[1] J. P. Schwanethal,[2] F. Postberg,[3] R. Srama,[3] S. Kempf,[3] G. Moragas-Klostermeyer,[3] J. A. M. McDonnell[1] and E. Grün[3,4]

[1] *Planetary and Space Sciences Research Institute, The Open University, Walton Hall, Milton Keynes MK7 6AA*
[2] *Department of Earth Sciences, The Open University, Walton Hall, Milton Keynes MK7 6AA*
[3] *MPI für Kernphysik, Saupfercheckweg 1, 69117 Heidelberg, Germany*
[4] *Hawaii Institute of Geophysics and Planetology, University of Hawaii, 1680 East West Road, POST 512c, Honolulu, HI 96822, USA*

Accepted 2007 March 8. Received 2007 March 8; in original form 2006 November 6

ABSTRACT

We present the first *in situ* direct measurement of the composition of particles in Saturn's rings. The Cassini cosmic dust analyser (CDA) measured the mass spectra of nearly 300 impacting dust particles during the 2004 October E ring crossing. An initial interpretation of the data shows that the particles are predominantly water ice, with minor contributions from possible combinations of silicates, carbon dioxide, ammonia, molecular nitrogen, hydrocarbons and perhaps carbon monoxide. This places constraints on both the composition of Enceladus, the main source of the E ring, as well as the grain formation mechanisms.

Key words: planets: rings – planets and satellites: individual: Enceladus.

1 INTRODUCTION

In contrast with Saturn's main 'icy' rings (A, B and C), whose brightness and optical depths make it possible to obtain good compositional information via reflectance spectroscopy (e.g. Poulet et al. 2003), the 'dusty' rings (in particular E and G) are extremely faint, with low optical depths. This makes obtaining reflectance spectra extremely difficult and consequently, until now, the composition of particles in the G and E rings has been inferred from the composition of the main rings and the composition of possible source moons. The size distribution of the dusty ring particles has been inferred from the slope of broadband photometric measurements (Nicholson et al. 1996), which are more sensitive to particle size distributions than composition. The narrow G ring has a neutral-red sloping spectrum, in common with most other dusty rings (see e.g. the recent Cassini measurements of the jovian rings by Throop et al. 2004), indicating a power-law size distribution. However, Saturn's E ring appears to be considerably different.

Telescopic (Showalter, Cuzzi & Larson 1991; De Pater et al. 1996; Nicholson et al. 1996; Bauer, Lissauer & Simon 1997) and spacecraft-based (Showalter et al. 1991; Meyer-Vernet, Lecacheux & Pedersen 1996) observations, as well as numerical modelling (Seidelmann, Harrington & Szebehely 1984; Showalter, Cuzzi & Larson 1991; Horányi, Burns & Hamilton 1992; Hamilton 1993; Juhász & Horányi 2004), indicate that Saturn's diffuse outer ring, the E ring, extends from 3 R_s (R_s, Saturn radius = 60 330 km) to >8.0–9.5 R_s. The E ring is believed to be at most 0.5 R_s thick, with a decrease in thickness (and corresponding increase in spatial density) at 3.95 R_s, coincident with the orbit of Enceladus (Showalter et al. 1991). This dynamical connection with Enceladus is reinforced by an apparent compositional link based on remote sensing, as the reflectance spectra of Enceladus and the E ring are similarly blue-sloping (Showalter et al. 1991; Nicholson et al. 1996). Further convincing evidence linking Enceladus with the E ring has been found recently by the Cassini cosmic dust analyser (CDA). Dust fluxes measured during a close Enceladus flyby (Spahn et al. 2006) (during which no high-resolution time-of-flight (TOF) spectra were obtained) and images taken by the ISS instrument (Porco et al. 2006) imply a significant dust source towards the southern pole of Enceladus. This appears to coincide well with a localized hot spot on Enceladus's surface, reported by the CIRS instrument (Spencer et al. 2006) and the VIMS instrument (Brown et al. 2006).

The aforementioned difficulty in remotely obtaining compositional information about E ring particles means that the results presented here are the first *in situ* measurements of the composition of any 'dusty' planetary ring. As well as the particles' composition we also present an initial analysis of the likely particle generation mechanisms and subsequent implications for the primary source, Enceladus.

1.1 Observations

The CDA chemical analyser (CA) subsystem (Fig. 1) returns mass spectra of impacting dust particles using a TOF technique. Dust particles impacting on to the rhodium chemical analyser target (CAT) create an impact cloud consisting of anions, cations, electrons, neutral atomic and molecular species and macroscopic ejecta. A strong electric field in the region (A in Fig. 1) of the impact point accelerates the cations towards a detector (the multiplier) via regions of

⋆E-mail: j.k.hillier@open.ac.uk

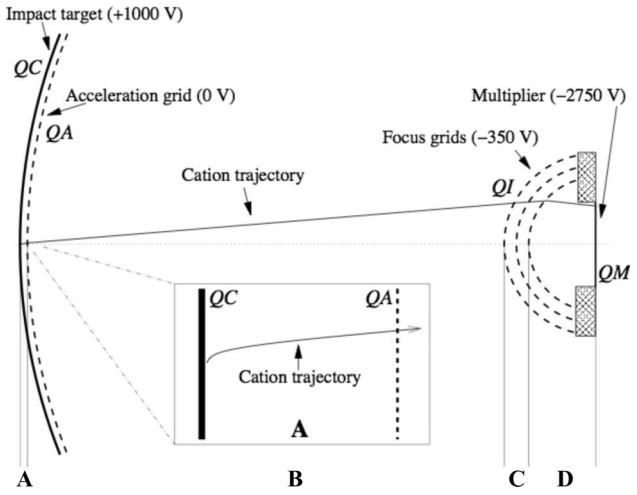

Figure 1. A 2D schematic of the Cassini CA subsystem. The four main field regions are shown (A, B, C, D), together with nominal instrument design voltages. The trajectory of a 'just detected' ion is indicated, with the inset diagram showing the ion behaviour within the acceleration region due to non-zero initial ion energy. Taken from Hillier et al. (2006).

varying field strengths (Fig. 1B–D, designed to help focus the ions on to the detector and then accelerate them on to the multiplier face plate). The electrons and anions are accelerated towards, and collected by, the CAT. Each impact on to the CAT is recorded via the four channels shown in Fig. 1: QC, the integrated charge signal from the negatively charged components of the impact cloud; QA, a single charge value representing the maximum number of positive ions created during the impact, generated by ions striking the acceleration grid; QI, the integrated charge signal generated by positive ions striking a grid situated just prior to the multiplier region – this signal, as the best indicator of the number of ions which subsequently form the mass spectrum, is used to calibrate the multiplier signal from volts to ion numbers; and finally QM, the aforementioned multiplier signal which forms the mass spectrum. The QM signal is a positive ion TOF spectrum, with a mass-dependent mass resolution (Srama et al. 2004; Postberg et al. 2006) of $(\Delta m/m) = 10$–50.

Conversion of the QM spectra from time to mass space is, in principle, simple (arrival time being proportional to the square root of the ion mass). In reality this process is complicated by the ions' initial velocity distribution, instrument geometry, plasma shielding effects and unknown precise impact times, which can broaden and shift peaks making calibration of spectra non-trivial (Hillier et al. 2006). The dominant uncertainty in determining the exact impact time (and hence the 'zero-point' of the mass scale) arises from the instrument triggering method. Post-impact recording is triggered by (pre-set) charge thresholds being exceeded on either the QC, QA, QI or QM channels. Recording triggered by the QC or QA channels will produce spectra that are more easily calibrated than those triggered by the QI or QM channels. In the former case, QC or QA triggering, the instrument records the arrival of all low-mass species present (e.g. H^+), whereas in the latter case, triggering by QI or QM, these earlier peaks are lost or truncated. Consequently, to convert the spectra from time-space to mass-space the source species of at least two peaks must be identified. This process involves estimating the likely trigger method based on charge levels and then looking for peaks at the 'expected' times for that particular triggering method. In cases where the ion species corresponding to at least two peaks can be identified unambiguously, or patterns typical of molecular clustering can be found, a mass scale can be derived. Care must then be taken when interpreting the mass spectra as the spectra may contain features due to projectile constituents, target constituents or recombinational products of the two. Just as the absence of a species in a spectrum does not necessarily mean the species is not present in the particle (many species prefer to form negative ions, or may recombine before they reach the multiplier), so it also should not be assumed that the presence of a polyatomic ion in a spectrum means the ion's parent species was present in the original dust particle.

Cassini's path during the ring plane encounters between 2004 October 25 and 30, and the positions at which CA spectra were obtained are shown in Fig. 2. The E ring shown in Fig. 2 is the 'classical' E ring – the extent of which has been determined from optical observations. The detection of gravitationally bound particles at distances from Saturn further than the outermost fringe of the 'classical' E ring implies that the E ring may be larger, although further measurements throughout the region are required before the E ring can be definitively stated to extend *continuously* as far as the 14.1 R_s shown here (Kempf et al. 2005a). However, to avoid confusion we will refer to all the particles discussed in this paper as belonging to the E ring. The possibility of ring particles being detected by the CA depends not only on the position and trajectory of Cassini, but also on the orientation of the instrument, as an impact on to the CAT occurs only if the incoming dust relative velocity vector is within $\pm 28^\circ$ of the nominal instrument boresight direction. Fig. 3 (lower panel) shows how the spectra obtained relate to the orientation of the CDA boresight with respect to bound, circularly orbiting particles in or near the ring plane.

The ascent through the ring plane on 2004 October 26 took place at 19.5 R_s, too far from Saturn for the detection of E ring particles, although several spectra characteristic of stream particles were detected (i.e. small charged dust particles accelerated within Saturn's magnetosphere to very high velocities Kempf et al. 2005b,c). Cassini then descended back through the ring plane at a distance of 8.1 R_s. On October 27, when the CAT orientation allowed detection of bound ring-plane particles, the dust impact rate increased substantially (Figs 2 and 3), and the spectra ceased to show 'stream' characteristics and instead began to show repetitive spectral peaks. These spectra show a range of peak widths that can, by measuring the mean full width half maximum of peaks in each spectrum, be broadly split into 'wide' and 'narrow' types (Fig. 4). A few spectra were also returned that are neither stream nor wide/narrow types but which, due to a lack of identifiable peaks or peak patterns (and the instrument triggering mechanism in some cases) are difficult if not impossible to calibrate. These are categorized as 'other' types. Cassini's positions when the four types of spectra were detected are shown in Fig. 3 (upper panel).

The repetitive features seen in the spectra obtained near the ring plane are similar to those seen in laboratory-based experiments with organic particles (Goldsworthy et al. 2002, 2003) and impacts on to water ice (Timmermann & Grün 1991), and are attributed to molecular cluster ions. Cluster spectra were detected from 23:44 SCET on October 27 until 12:13 SCET on 2004 October 29, corresponding to radial distances of 8.1–14.1 R_s from Saturn and 1.63–2.24 R_s out of the ring plane, respectively (the closest approach to Saturn during this time was 6.16 R_s). Fig. 5 shows examples of both narrow (i, ii, iii) and wide (iv) cluster spectra.

2 RESULTS AND ANALYSIS

Instrument sampling for cluster spectra was triggered by the QM channel, truncating or removing the first spectral peak, and complicating calibration on to a mass scale. The minimum atomic

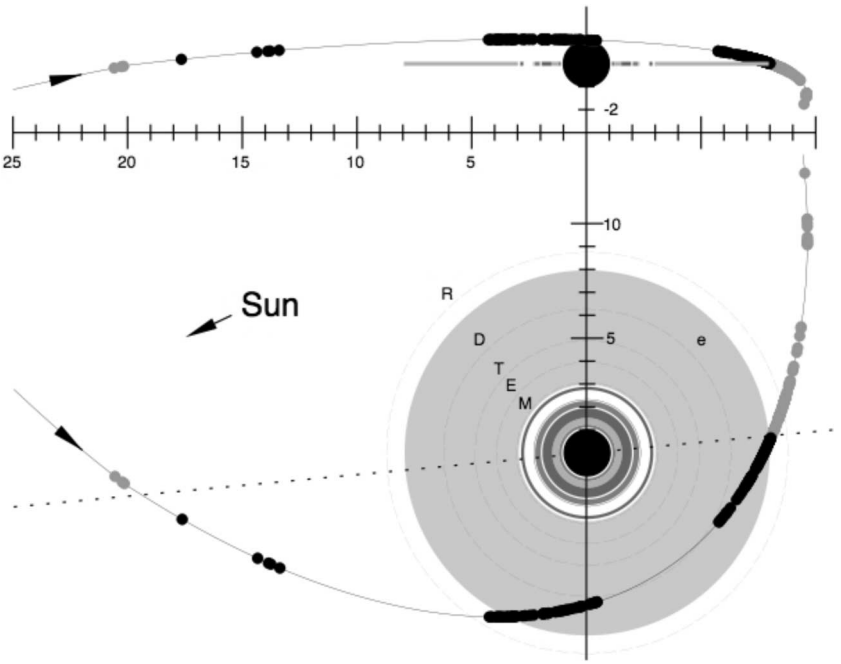

Figure 2. Cassini's path between 2004 October 25 and 30. The orbits of the moons Mimas (M), Enceladus (E), Tethys (T), Dione (D) and Rhea (R) are shown, together with the inner rings and the 'classical' diffuse E ring (e). Dust impacts on the CDA instrument which resulted in spectra are shown by the black circles (above ring plane) and the grey circles (below ring plane). Axis units are Saturn radii (R_s).

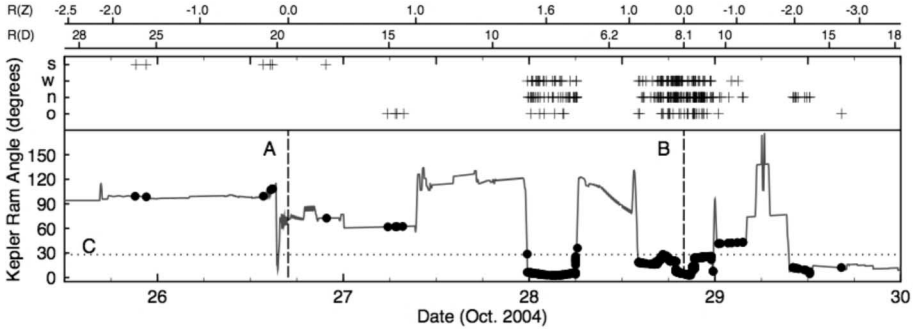

Figure 3. CDA pointing history and detection of impact spectra. The upper panel shows the times of detection of the different spectral types: stream (s), wide-peaked cluster (w), narrow-peaked cluster (n) and other (o) spectra showing either no peaks or peaks which are as yet unidentified. The lower panel shows the angle between the boresight of the CDA instrument and the apparent incoming velocity vector of dust particles in bound, circular orbits. Spectrum-generating impacts are shown by the black circles. The times of the ascending (A) and descending (B) ring plane crossings are also shown, together with the instrument field of view (C) for direct impacts on to the CAT – impacts indicated above this line can only be generated by dust particles with non-zero eccentricities or inclinations. The scale bars show the distance from Saturn [R(D), in R_s] and the vertical distance from the ring plane [R(Z), also in R_s].

mass corresponding to the first peak present in the majority of the cluster spectra is 18–19 a.m.u., assuming the trigger peak is due to H^+ (which is almost always the case). The two obvious candidate species with these masses are $(NH_3)H^+$ (ammonium ions) and $(H_2O)H^+$ (hydronium ions). Hydronium ions may have already been observed in stream particles (Kempf et al. 2005c), and water ice dominates the surfaces of Enceladus (Cruikshank et al. 2005; Emery et al. 2005), Tethys (Cruikshank et al. 2005; Emery et al. 2005), Rhea (Cruikshank et al. 2005; Emery et al. 2005) and Dione (Buratti et al. 2002; Cruikshank et al. 2005) amongst others. Furthermore, pure ammonia ice particles are unlikely to exist for long as E ring particles, due to their volatility (e.g. Brown 2000) and subsequent increased sensitivity to sputtering processes (Jurac, Johnson & Richardson 2001). In addition, ammonia compounds, suggested as a possible agent for cryovolcanism on Enceladus (Kargel & Pozio 1996), have only been detected as trace components on the surface of Enceladus (Emery et al. 2005), barely detected in the plume emanating from the southern polar region of Enceladus (Waite et al. 2006) and only possibly detected in stream particles (Kempf et al. 2005c). If both ammonium and hydronium ions are present then we would expect to be able to resolve both peaks. As only one peak is present in the majority of spectra, it is undoubtedly due to hydronium and hence water ice. Calibration of the spectra on to a mass scale, with the first two possible cluster peaks assigned to $(H_2O)H^+$ and $(H_2O)_2H^+$, shows that the remaining peaks correspond very well to $(H_2O)_jH^+$ ($j > 2$). The water cluster peaks show no evidence of 'magic number' clustering (Wróblewski et al. 2001) in those spectra where the peaks are clearly resolved, although 'contaminants' (e.g. possible, but undetectable, Fe contributions to the $(H_2O)_3H^+$ peak) complicate the relative peak proportions. Fig. 5

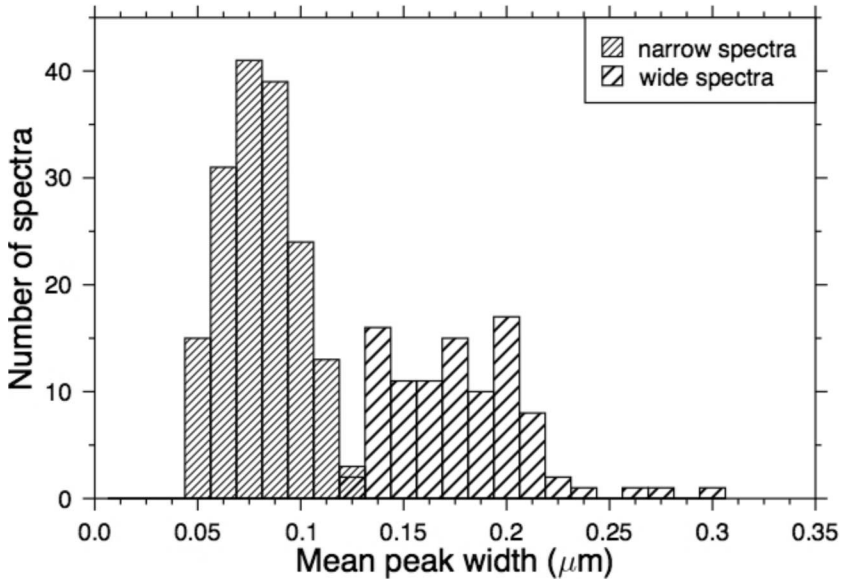

Figure 4. A histogram showing the variation in the mean widths of peaks in the mass spectra. The small minimum at 0.125 μs is used to define the boundary between the 'wide'- and 'narrow'-type spectra.

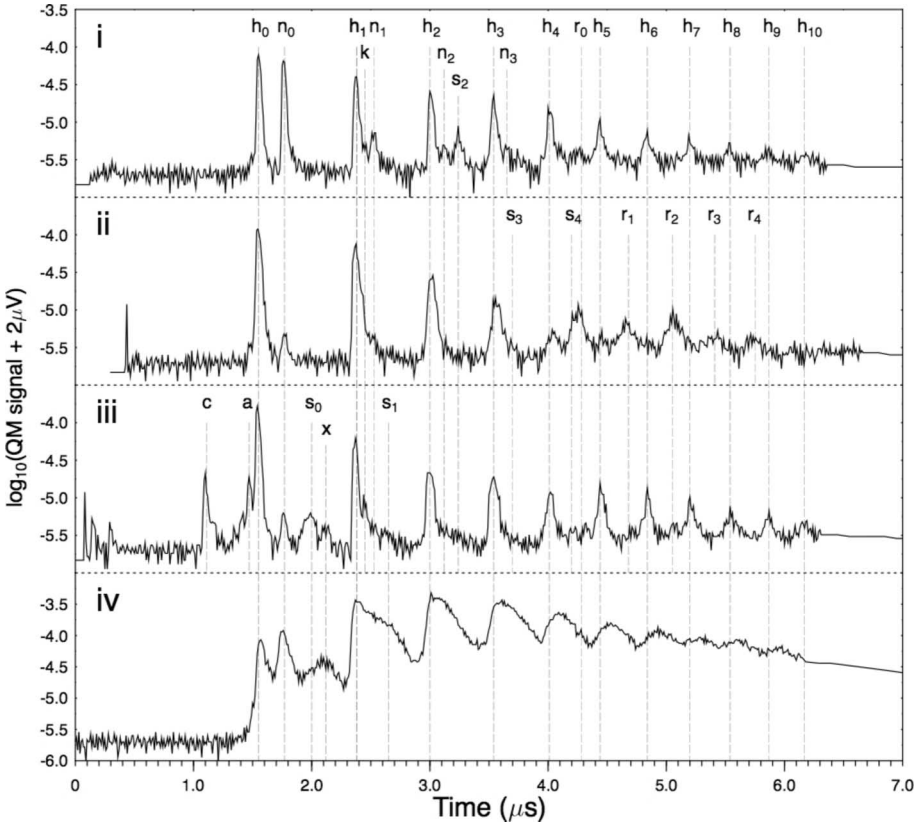

Figure 5. Examples of mass spectra obtained in the Saturnian system. Panels (i), (ii) and (iv) show typical narrow (i), (ii) and wide (iv) spectra from CDA. Panel (iii) shows the single narrow-type spectrum in this data set which has pre-hydronium peaks. The spectra are aligned on the hydronium peak. The peak labels are explained within the main text.

shows examples (i–iii) of narrow-type spectra including an example (iii) of a cluster spectrum with identifiable pre-$(H_2O)H^+$ peaks.

In these narrow-type spectra we regularly observe: water–water clusters (h_{1-10} in Fig. 5), often sodium (n_0) and simple sodium–water clusters (n_{1-3}), as well as the more complex cluster Na_2OH^+ at 63 a.m.u. (s_2); and sometimes observe: potassium (k in panel i of Fig. 5) in small amounts (although rarely potassium–water clusters as the mass resolution decrease means separating the cluster peak from the 55 a.m.u. $(H_2O)_3H^+$ (h_2) cluster peak is extremely difficult), carbon (c in panel iii of Fig. 5) together with possible CH^+

(1.17 μs) rhodium (r_0) and rhodium–water clusters ($r_{1–4}$). The target signature, rhodium, is less apparent in the spectra than expected from laboratory iron–particle calibration. However, as the energy transfer between the impacting dust particle and the target is related to the ratio of their densities (Stübig 2002) this implies that the dust particles have a lower density, consistent with water ice. In spectra with a definite rhodium peak, rhodium–water clusters of up to four water molecules have been seen (e.g. Fig. 5ii). Target-projectile cluster ions such as these have been previously observed in both laboratory spectra (Stübig 2002) and flight spectra – RhSi in stream particles (Kempf et al. 2005c) and RhFe in interplanetary dust particles (Hillier et al. 2007) for example – but not to such an extent. Previous reports of both sodium and potassium in CDA spectra have attributed them both to surface contaminants of the rhodium target, appearing in stream-type spectra at a rate that was in agreement with the expected area of surface contamination (Kempf et al. 2005c) and also (particularly in the case of sodium), as particle constituents (Postberg et al. 2006). Postberg et al. investigated the composition of jovian stream particles, and showed that those particles do contain a large amount of sodium, statistically in excess of that expected from target contamination. The E ring particle spectra discussed here do exhibit sodium features, but at a frequency that is consistent with sodium target contamination.

In one spectrum (Fig. 5iii) we see a small peak at 18 a.m.u. (labelled 'a', at ∼1.45 μs), possibly due to the ammonium ion $(NH_3)H^+$, although this peak could also be due to the H_2O^+ ion observed in SIMS experiments on water ice films (e.g. Donsig & Vickerman 1997). Donsig & Vickerman (1997) give the ratio of $(H_2O)H^+$ to H_2O^+ as approximately six, which would result in a larger 18 a.m.u. peak than we observe here, although we cannot discount H_2O^+ as the cause of the 18 a.m.u. peak. Work is currently ongoing to determine how the ratio of the number of ions in the 18 a.m.u. peak to the number of ions in the hydronium peak varies with impact velocity and particle mass, in an attempt to definitively identify the peak. The remaining unidentified peaks in Fig. 5 are denoted by s_0 (approximately 28 a.m.u., at 2.0 μs), x (approximately 31 a.m.u., at 2.12 μs), s_1 (approximately 42–44 a.m.u., 2.66 μs – from this sample of spectra no obvious candidates for species at 42 and 43 a.m.u. present themselves, and we will instead concentrate on contributions to this peak from 44 a.m.u. species, for which there are several candidates), s_3 (approximately 79 a.m.u., 3.7 μs) and s_4 (approximately 97 a.m.u., 4.2 μs). Of these, the peak at ∼31 a.m.u. is most easily identified, as a water–carbon cluster [$C(H_2O)^+$ and $C(H_2O)H^+$]. This cluster appears to contribute, together with s_0, to the wide peak shown in Fig. 5(iv), but as carbon is a known contaminant of the CAT, we cannot determine whether the C^+ is from the impacting dust grain or the rhodium target. The ratio of 27–31 a.m.u. ions to the total number of ions in a spectrum for the E ring spectra is ∼0.01–0.03, implying a ratio of these species to water in the original dust particles of at least this value. To try to identify peaks s_0, s_1, s_3 and s_4 we examine the possible candidates already known to or suspected to occur on or near Enceladus, choosing two discrete families of source species: mineralogical (Si-based refractory compounds) and volatile (CHON-based compounds).

Stream particles, detected before Saturn orbit insertion, but possibly originating from the E ring (as well as the A ring) (Kempf et al. 2005b) have been shown to contain small amounts of silicon (Kempf et al. 2005c). Si (28 a.m.u.) would be expected to come from any silicates present and may be accompanied by SiO^+ (44 a.m.u.) and even perhaps SiO_2^+ (60 a.m.u.) although predicting the relative ion abundances between these species is non-trivial. These silicon-based species, together with associated water clusters may explain peaks s_0 (Si^+), s_1 [44 a.m.u.: SiO^+, possibly minor $Si(H_2O)^+$], some s_2 [62 a.m.u.: $SiO(H_2O)^+$, 63 a.m.u.: $SiO(H_3O)^+$] although this peak is probably dominated by the sodium–water cluster mentioned previously, s_3 [79 a.m.u.: $SiO_2(H_2O)H^+$, 81 a.m.u.: $SiO(H_2O)_2H^+$] and s_4 [97 a.m.u.: $SiO_2(H_2O)_2H^+$]. These species represent a mineralogical explanation to the s_n peaks.

Other possible component species, from more 'volatile' parents, can only be considered following the publication of plume vapour mass spectra by the INMS instrument on Cassini (Waite et al. 2006). The INMS found that the vapour was 91 ± 3 per cent H_2O, 3.2 ± 0.6 per cent CO_2, 4 ± 1 per cent N_2 (or CO) and 1.6 ± 0.4 per cent CH_4. Other trace (<1 per cent) species detected were NH_3 (<0.5 per cent), C_2H_2, HCN and C_3H_8. Of these species CO^+ (28 a.m.u.) (or HCO^+ at 29 a.m.u.) and N_2^+ (28 a.m.u.), together with HCN^+ (27 a.m.u.) may form, or contribute to peak s_0. Similarly, CO_2^+ (44 a.m.u.) and $C_3H_7^+$ (43 a.m.u.), together with $HCN(H_2O)H^+$ (46 a.m.u.) or possibly CO–water or N_2–water clusters (46–47 a.m.u.) may explain possible contributions to peak s_1. Peaks s_2 [e.g. $CO_2(H_2O)H^+$ at 63 a.m.u.], s_3 [e.g. $CO_2(H_2O)_3H^+$ at 81 a.m.u.] and s_4 [e.g. $CO_2(H_2O)_3H^+$ at 99 a.m.u.] then form by further, but less likely, clustering of the s_0 and s_1 species with water. Additionally, ions from CO_2-derived species such as carbonic acid (H_2CO_3, 62 a.m.u.) may be present.

Interestingly, given the presence of both N_2 (presumably derived from NH_3) and CO_2 in the plume vapour, and hence presumably within Enceladus itself, ions derived from possible reaction products of NH_3 and CO_2 such as ammonium carbonate [$(NH_4)_2CO_3$, 96 a.m.u.] or ammonium hydrogen carbonate (NH_4HCO_3, 79 a.m.u.), together with further water clusters, provide less-likely but possible explanations for the s_3 and s_4 peaks. However, it is important to note that the number of NH_4^+ ions produced as breakdown products of these species would probably be higher than the trace amounts possibly detected here. From this small sample, and without a more detailed statistical investigation into the occurrence of, and correlations between, the s_0, s_1, s_2, s_3 and s_4 peaks (currently under way; Postberg et al. 2007), a definite conclusion as to the identity of their parent species is not yet possible and instead we will later concentrate on possible dust formation mechanisms which would produce particles with compositions based on either the mineral, volatile or possibly both, explanations given above.

The final type of spectrum that we have yet to consider is the 'wide' type. The wide spectra (Fig. 5iv) show similar clustering to the narrow spectra, although cluster peaks may swamp smaller peaks. The s_0/x peaks are often more apparent in the wide spectra although this may be an observational effect from the increased overall ion numbers in these spectra. In addition the peak maxima are progressively shifted from their expected positions to slightly later arrival times, which implies that shielding and delayed cluster ionization are occurring in the impact plasma. One might therefore expect the occurrence of 'wide'-type spectra to be correlated with impact plasma density. Plasma shielding is dependent on the plasma temperature and charge density (assuming local thermodynamic equilibrium) and hence the impacting particle's mass and impact speed. The total number of electrons detected by the CAT (the QC signal), which is also a function of particle mass and impact speed, does not show a strong correlation with wide-type spectra (Fig. 6), although no wide spectra are found for impacts with low total charge production.

The impact speed calibration used in this paper is derived specifically for impacts on the CAT and is based on an empirical relationship between the QC signal rise-time and impact speed from laboratory impacts. There is an uncertainty of a factor of 1.6 for any

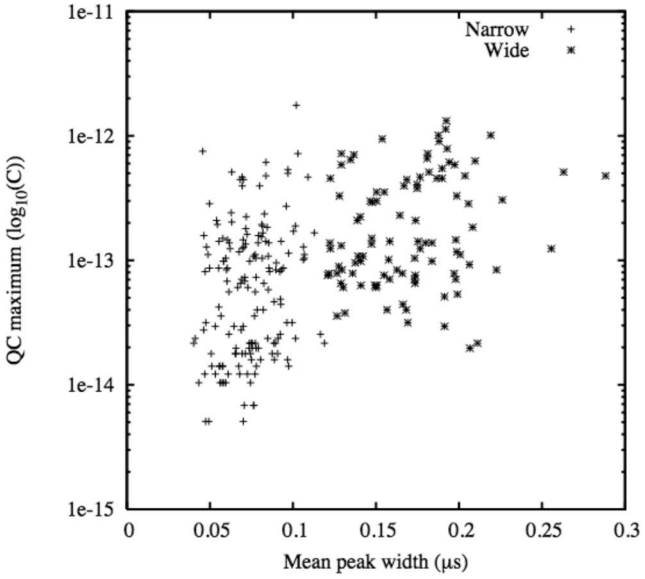

Figure 6. The maximum (integrated) anion signal (QC) from the CAT plate as a function of the mean spectral peak width.

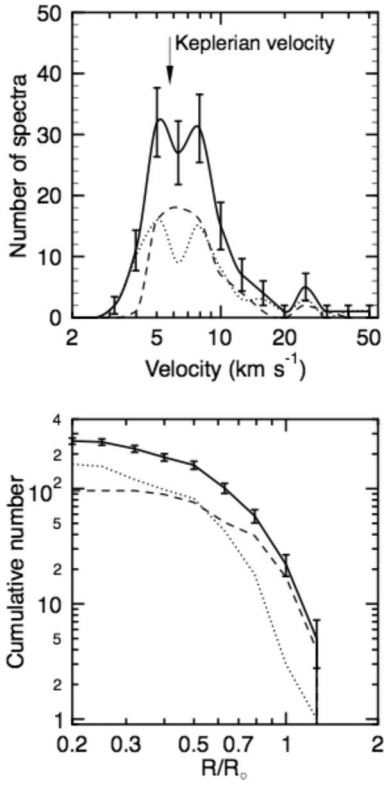

Figure 7. The derived velocity (upper panel) and radius (lower panel) distributions for the water-rich particles detected by CDA. The distributions are shown for wide-type (dashed line) and narrow-type (dotted line) particles, as well as the total (solid line). The radii are calculated from particle masses derived assuming a density of ice, a circular Keplerian velocity and laboratory calibration for iron particles. The results are presented here as a cumulative size distribution (relative to a nominal size of $R_0 = 1$ μm, which may have a systematic error due to the uncertainty in the application of laboratory calibration to ice particles).

individual impact velocity. A Gaussian fit to the main peak in the impact speed distribution shown in Fig. 7 results in a mean impact speed of 6.4 ± 0.2 km s^{-1}, which is close to the expected mean impact velocity, for circular Keplerian orbits, of 5.76 km s^{-1} (arrowed in Fig. 7). (The overall mean impact speed of 7.7 km s^{-1} results from the contribution of small particles detected on apparently unbound orbits.) The slightly higher peak impact speed may be due to particles in eccentric or inclined orbits or may be an observational bias resulting from the speed dependence of impact plasma production ($QC = km^{\alpha}v^{\beta}$ where α and β, whilst varying with impacting particle composition, are typically 1 and 3–4, respectively). The range of derived speeds (obtained via a Gaussian fit to the main peak) is a factor of 1.4, slightly less than the expected uncertainty from laboratory data for each individual speed. This scatter in impact speeds is therefore too large to allow us to determine whether there is any distribution in the particles' eccentricities, although we should be able to tell whether a particle is in a bound or unbound orbit. We therefore assume circular Keplerian orbits when deriving particle masses. The lack of a strong bimodality in the derived impact speeds indicates that any plasma shielding or delayed clustering effects responsible for some widening of the peaks may be due to a variation in the masses (and hence radii) of the particles. This does indeed appear to be the case, as shown in the lower panel of Fig. 7, with wide peaked spectra most often due to larger or more massive particles.

No differences in the production of wide- or narrow-type spectra with ring plane position or Saturnian distance are apparent (Fig. 3, upper panel), indicating that, excluding possible mass effects, either the wide- and narrow-type spectra are due to particles of similar composition or the E ring is extremely well mixed. The overlap in the magnitude of the QC signals between spectra with similar mean peak widths (Fig. 6) indicates that plasma shielding may not be the only factor in widening spectral peaks. Delayed clustering and ionization in a neutral-rich impact vapour cloud (for wide peaked spectra with low maximum QC signals), together with rapidly dissipating plasma (for narrow-peaked spectra with high maximum QC signals) may however, still explain this effect.

3 DISCUSSION

The CA detected bound particles of apparently similar composition in or near the ring plane, between 8.1–14.1 R_s, and up to 2.3 R_s out of the plane. The elemental composition of these particles represents the composition of their parent bodies, although some components may be lost or depleted during the ejection process and any subsequent weathering by plasma sputtering. Whilst we cannot currently reliably discriminate between mineralogical or volatile components in the E ring particles detected by the CA, the presence of silicates or extremely volatile compounds, and perhaps trace amounts of ammonia, can be used to place constraints on the source body (or bodies) and the ejection mechanism responsible for dust creation and replenishment into the E ring.

Making the assumption that Enceladus is the sole source of the dust we have detected we now consider possible particle generation mechanisms, which may result in particles which produce 'mineral' or 'volatile' CA mass spectra. First, in Fig. 8, we consider the case where the spectra are silicon-rich. The dust source regions are then divided into two types: regions with and regions without appreciable amounts of ammonia. In each region there are two possible ejection mechanisms: volcanism and impacts. Volcanism encompasses both 'active' volcanism, such as geysers or venting and more 'passive' volcanism involving warm upwelling and sublimation/condensation mechanisms to generate the dust. The most likely routes for particle

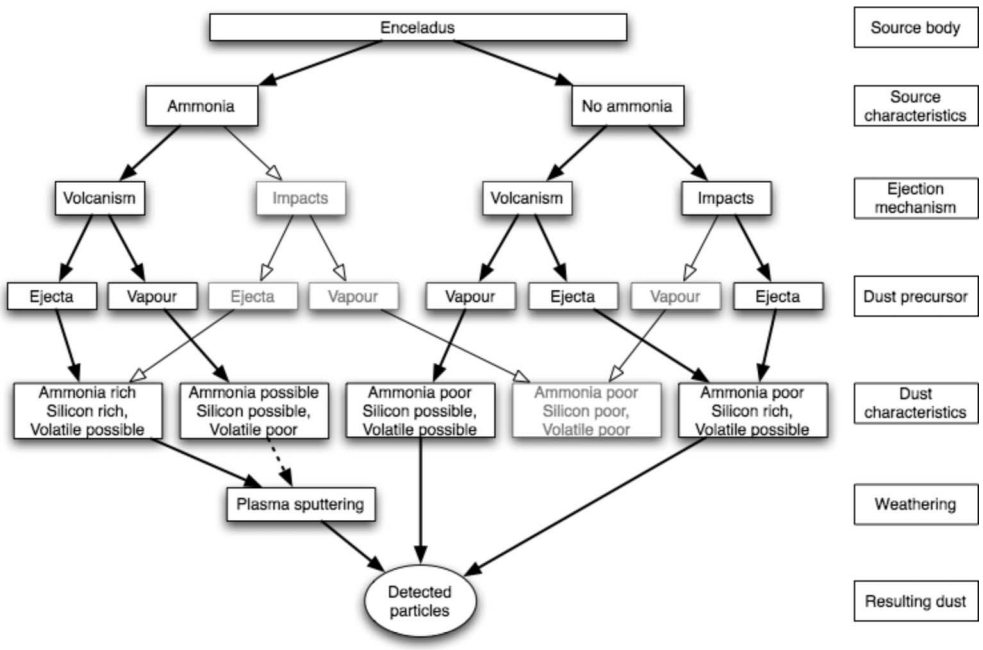

Figure 8. Possible generation mechanisms for E ring particles that result in dust with the chemical properties we observe. The diagram is described in detail in the main text.

production are shown in black, with those less likely to produce the types of particles we observe shown in light grey. A dashed line indicates a route that is likely for one particle composition but not for another.

Both volcanism and impact processes generate precursors to the dust we observe, in the form of direct macroscopic ejecta and/or vapour. The dust produced can then be characterized by the abundances of silicon and ammonia that it is likely to contain. As remote observations have indicated that there is little ammonia ice present on a large scale across Enceladus (Emery et al. 2005), we can limit the likely location of surface or near-surface ammonia to cracks on the surface such as those in the southern polar regions. This represents a small surface area for impact-generation of a large number of dust particles. The warm southern polar regions are also the location of the observed 'volcanic' activity, which is more likely with ammonia-rich materials than for pure water ice, although pure water ice volcanism may still occur. Most of the rest of the surface of Enceladus appears to be pure water ice and is more likely to be involved in impact-generation processes rather than volcanism. We therefore discount impacts in the potentially ammonia-rich regions as a mechanism for appreciable dust formation. The condensation of impact-generated vapour is unlikely to be able to coat lofted silicate particles with appreciable amounts of ice. However, impact ejecta, volcanic ejecta and (with suitable updraughts) vapour should all be able to form ice-rich dust that contains silicon. Direct implantation of interstellar (ISD) or interplanetary (IDP) dust grains, rich in silicates, into E ring particles is unlikely given the extremely low spatial density of the E ring and the relatively short dynamical lifetimes of the grains (Burns & Gladman 1998; Jurac et al. 2001). Although no silicates have been clearly detected in reflectance spectra of Enceladus (or the other icy moons Buratti et al. 2002; Cruikshank et al. 2005; Emery et al. 2005), they are almost certainly implanted on to the surface by ISD and IDP grains and, if present in the observed plumes, via ballistic trajectories back on to the surface of Enceladus. Also, regardless of the generation mechanism, Enceladus must act as a sink to E ring particles, which will then distribute silicate-containing particles across the surface, although the spectral signatures of these grains may be masked by water vapour condensates. However, if the interior of Enceladus consists of a small rocky core surrounded by a still-liquid ammonia–water mixture then the extremely basic environment and high pressures will leach minerals from the core, bringing some silicon into suspension and providing a possible source for the silicon observed in the E ring particles. If Enceladus is undifferentiated then the silicon should still be present but may be in a more macroscopic form.

Similar particle generation routes are shown for the 'volatile'-rich case in Fig. 8. The same ammonia-rich and -poor region arguments as for the silicate paths are valid but now we must consider the likely loss mechanisms rather than the retention mechanisms considered for the silicates. Macroscopic ejecta routes, from impacts or 'active' volcanism should all preserve some volatile compounds within the generated grains, whereas vapour condensation methods should preferentially deplete or remove these compounds.

Although not shown on Fig. 8, a third possible generation method for these dust grains exists which spans both the volcanism vapour and ejecta methods. The laboratory study of adsorbed gas release from water ice (e.g. Bar-Nun et al. 1985, 1987; Hudson & Donn 1991; Ayotte et al. 2001) shows that, for a variety of gases (Ar, N_2, O_2, CO, CO_2, CH_4), gas release occurs numerous times at temperatures below that at which water starts to sublimate. Part of this process is believed to be related to the changes in the structure of water ice from amorphous to cubic to hexagonal, followed by the sublimation of gas clathrate hydrates. Interestingly, the desorption of several gases (Ar, CO, N_2 and CH_4) was accompanied by the ejection of large quantities of 0.1–1 μm radius ice grains (constituting tens of percent of the original water mass) (Bar-Nun et al. 1985, 1987). This ejection occurred at temperatures of ∼40, ∼170 and ∼180 K (Bar-Nun et al. 1985), with the smaller dust grains expelled at speeds greater than 1.67 m s^{-1}. (For comparison, the escape velocity from Enceladus is ∼250 m s^{-1}, which means that unless the clathrate breakdown grain ejection speeds were *much* greater than 1.67 m s^{-1}, this dust production method is unable to directly eject

grains into the E ring, as suggested by Bar-Nun et al. (1985). It is instead likely that gas drag within the vapour plumes delivers particles into the E ring.) In the higher temperature ranges, particles as large as 0.1 mm are expelled. In at least the case of Ar the grain emission can occur for up to 6 h without an increase in temperature beyond that required to start the process; the emission then slows and a small increase in heat restarts it, with emission continuing this way until the available Ar is exhausted. Given the apparent gas composition of Enceladus's plume (Waite et al. 2006) it is possible that similar gas desorption mechanisms may be occurring within the 'Tiger stripes' on Enceladus (suggested in Bar-Nun et al. 1985), creating dust which can act as condensation seeds in vapour whilst allowing the trapping and emission of some volatiles or silicates but not requiring highly active venting and near surface liquid. We note that this process has also been suggested independently by Kieffer et al. (2006), although they postulate the sublimation of the small ejected particles to produce the observed vapour densities, rather than the 'seeding' of the vapour with condensation cores.

Finally, as the dust discussed here was detected at large distances from Enceladus it is likely to have undergone plasma sputtering in the energetic plasma environment around Saturn, resulting in the preferential loss of ammonia (and to a lesser extent water) from the dust particles. If Enceladus is the source of *all* our detected particles, then a transport mechanism to large Saturnian distances, applicable to particles with a low surface charge, is required. (The particles producing the ∼300 spectra were not detected by the CDA entrance grid system, implying low electrostatic potential, based on the derived radii of the particles.) The timescale of this mechanism must be commensurate with the short lifetime (potentially just 50 yr, depending on the plasma conditions) of the particles (Burns & Gladman 1998; Jurac et al. 2001). If the particles are produced by moons in orbits closer to the detection positions of the grains (e.g. Rhea, Dione or Tethys) then we may be able to distinguish the sources by comparing the grain spectra. In the case of Tethys, suggested as a possible dust source (Hamilton 1993; Juhász & Horányi 2004), the similarity of its reflectance spectrum with those of Dione and Enceladus (Cruikshank et al. 2005), and hence the expected similarity of mass spectra from dust from these objects, makes the reliable identification of the source body extremely difficult. If Rhea is a significant source then the expected presence of tholins (as indicated by the modelling of reflectance spectra by Cruikshank et al. 2005) in the dust grains should allow us to distinguish those particles it emits. The absence of spectral signatures commensurate with complex organics in the spectra discussed here indicates that Rhea is probably only a minor contributor of particles to the E ring, if at all.

4 CONCLUSIONS

We have presented the first direct *in situ* measurement of the composition of Saturn's E ring. The TOF mass spectra of grains are dominated by clusters from water ice. The spectra are characterized by the shape of the water cluster features as either 'wide' or 'narrow'. The wide spectra appear to result from grains that are more massive and there is no evidence, from this data, for differences in composition between the types. Other constituents of the grains include possible combinations of silicates, carbon dioxide, ammonia, molecular nitrogen, hydrocarbons and perhaps carbon monoxide.

Following consideration of the possible sources of the E ring particles, we have identified several potential routes, including explosive clathrate breakdown, to produce the dust we observe in the E ring, depending on the likely dust composition. For silicate-containing particles there are: volcanism in ammonia-rich regions, volcanism in ammonia-poor regions (less likely) and impact ejecta in ammonia-poor regions. For particles containing volatiles the likely routes are via mechanisms which produce larger initial particles – volcanic and impact ejecta or vapour phase formation combined perhaps with particles from clathrate breakdown. It is, however, likely that more than one of these processes plays a part on Enceladus. A larger sample of spectra (Postberg et al. 2007), together with further observations of Enceladus's plume and surface composition in the future may help more accurately determine the dominant sources and allow a more definitive interpretation of the CDA spectra.

ACKNOWLEDGMENTS

JKH, SFG, NM, JPS and JAMM acknowledge the financial support of PPARC. JKH thanks S. Sestak (Open University) for useful discussions. The authors acknowledge the work of P. Ratcliff in the early development of the CA and thank the referee N. Altobelli for his helpful comments. This work has made use of NASA's Astrophysics Data System.

REFERENCES

Ayotte P., Smith R. S., Stevenson K. P., Dohnálek Z., Kimmel G. A., Kay B. D., 2001, J. Geophys. Res., 106, 33387
Bar-Nun A., Herman G., Laufer D., Rappaport M. L., 1985, Icarus, 63, 317
Bar-Nun A., Dror J., Kockavi E., Laufer D., 1987, Phys. Rev. B, 35, 2427
Bauer J., Lissauer J. J., Simon M., 1997, Icarus, 125, 440
Brown M. E., 2000, AJ, 119, 977
Brown R. H. et al., 2006, Sci, 311, 1425
Buratti B. J., Hicks M. D., Tryka K. A., Sittig M. S., Newburn R. L., 2002, Icarus, 155, 375
Burns J. A., Gladman B. J., 1998, Planet. Space Sci., 46, 1401
Cruikshank D. P. et al., 2005, Icarus, 175, 268
De Pater I., Showalter M. R., Lissauer J. J., Graham J. R., 1996, Icarus, 121, 195
Donsig H. A., Vickerman J. C., 1997, J. Chem. Soc. Faraday Trans., 93, 2755
Emery J. P., Burr D. M., Cruikshank D. P., Brown R. H., Dalton J. B., 2005, A&A, 435, 353
Goldsworthy B. J. et al., 2002, Adv. Space Res., 29, 1139
Goldsworthy B. J. et al., 2003, A&A, 409, 1151
Hamilton D. P., 1993, Icarus, 101, 244
Hillier J. K., McBride N. M., Green S. F., Kempf S., Srama R., 2006, Planet. Space Sci., 54, 1007
Hillier J. K. et al., 2007, Icarus, in press
Horányi M., Burns J. A., Hamilton D. P., 1992, Icarus, 97, 248
Hudson R. L., Donn B., 1991, Icarus, 94, 326
Juhász A., Horányi M., 2004, Geophys. Res. Lett., 31, L19703
Jurac S., Johnson R. E., Richardson J. D., 2001, Icarus, 149, 384
Kargel J. S., Pozio S., 1996, Icarus, 119, 385
Kempf S., Beckmann U., Burton M., Helfert S., Srama R., Moragas-Klostermeyer G., Roy M., Grün E., 2005a, AGU Fall Meeting Abstracts, D5
Kempf S., Srama R., Horányi M., Burton M., Helfert S., Moragas-Klostermeyer G., Roy M., Grün E., 2005b, Nat, 433, 289
Kempf S. et al., 2005c, Sci, 307, 1274
Kieffer S. W., Lu X., Bethke C. M., Spencer J. R., Marsak S., Navrotsky A., 2006, Sci, 314, 1764
Meyer-Vernet N., Lecacheux A., Pedersen B. M., 1996, Icarus, 123, 113
Nicholson P. D. et al., 1996, Sci, 272, 509
Porco C. C. et al., 2006, Sci, 311, 1393
Postberg F., Kempf S., Srama R., Green S. F., Hillier J. K., McBride N., Grün E., 2006, Icarus, 183, 122
Postberg F. et al., 2007, Icarus, submitted

Poulet F., Cruikshank D. P., Cuzzi J. N., Roush T. L., French R. G., 2003, A&A, 412, 305
Seidelmann P. K., Harrington R. S., Szebehely V., 1984, Icarus, 58, 169
Showalter M. R., Cuzzi J. N., Larson S. M., 1991, Icarus, 94, 451
Spahn F. et al., 2006, Sci, 311, 1416
Spencer J. R. et al., 2006, Sci, 311, 1401
Srama R. et al., 2004, Space Sci. Rev., 114, 465
Stübig M., 2002, PhD thesis, Univ. Heidelberg
Throop H. B., Porco C. C., West R. A., Burns J. A., Showalter M. R., Nicholson P. D., 2004, Icarus, 172, 59
Timmermann T., Grün E., 1991, in Levasseur-Regourd A. C., Hasegawa H., eds, Origin and Evolution of Interplanetary Dust. Kluwer, Dordrecht, p. 387
Waite J. H. et al., 2006, Sci, 311, 1419
Wróblewski T., Gazda E., Mechlińska-Drewko J., Karwasz G. P., 2001, Int. J. Mass Spectrosc., 207, 97

This paper has been typeset from a MS word file prepared by the author.